NASA Technical Memorandum 80189

WIND-TUNNEL INVESTIGATION OF THE FLOW CORRECTION FOR A MODEL-MOUNTED ANGLE OF ATTACK SENSOR AT ANGLES OF ATTACK FROM -10^0 TO 110^0

THOMAS M. MOUL

NOVEMBER 1979

National Aeronautics and Space Administration
Langley Research Center
Hampton, Virginia 23665

WIND-TUNNEL INVESTIGATION OF THE FLOW CORRECTION FOR A MODEL-MOUNTED ANGLE OF ATTACK SENSOR AT ANGLES OF ATTACK FROM -10° TO 110°

By

Thomas M. Moul

SUMMARY

A wind tunnel investigation has been conducted to establish the flow correction, over a large angle of attack range, necessary to correct the measurements of an angle of attack sensor. The sensor was mounted ahead of the wing of a 1/5-scale model of a general aviation airplane. The investigation was preliminary, testing the effects of the spanwise and chordwise location of the sensor on the flow correction. The tests were conducted over an angle of attack range from -10° to 110°.

The tests showed the flow correction was substantial at all of the sensor locations tested, reaching over 15° at an angle of attack of 90°. The flow correction was found to increase as the sensor was moved closer to the wing (at a fixed spanwise location) or closer to the fuselage (at a fixed chordwise location). The experimentally determined slope of the flow correction versus the measured angle of attack below the stall angle of attack agreed closely with the slope of flight data from a similar full scale airplane. However, more tests should be conducted to investigate the observed bias between the two curves.

INTRODUCTION

In flight test investigations, it is often desirable to reduce the flight data to a form that can be compared directly with wind tunnel results or theoretical predictions. An essential flight quantity for this comparison is the true angle of attack of the airplane. One type of angle of attack sensor which has had widespread use is a vane which is usually mounted in front of the wing near the wing tip (see, e.g., the sensor in ref. 1). However, such a device only measures the local flow direction at the sensor, and to determine the true angle of attack of the airplane, corrections must be applied to this measured local flow direction (called the measured angle of attack herein). One correction to be applied to the measured angle of attack is a flow correction to account for the change in the flow direction due to

the presence of the airplane. Other corrections (for example, to account for airplane rotation) should also be applied to the angle of attack measured in flight (refs. 2, 3, and 4), but these corrections are not considered in this paper.

For airplanes in the normal, unstalled flight regime this flow correction can be and has been determined both experimentally and theoretically (refs. 2, 3, 5, and 6). Nevertheless, very little work has been done in determining the flow correction for flight at angles of attack above the stall. However, NASA Langley Research Center is investigating the stall/spin problem in general aviation airplanes and at the large angles of attack encountered in stalled or spinning flight the flow correction may be substantial. Consequently, if the flow correction is in fact large, it should be applied to the data taken during the stall/spin flight tests to enable direct comparison of the flight data with data from other sources (ref. 7).

This paper is a presentation of an exploratory investigation, using a 1/5-scale model of a low-wing general aviation airplane, into the nature of the static flow corrections necessary to correct the measurements of a vane angle of attack sensor over a large angle of attack range. These results can be used to obtain a flow correction to be applied to the angle of attack data taken on a full-scale research airplane during spin maneuvers (ref. 8).

In the present investigation the flow correction for the model was determined at four spanwise locations and at two chordwise positions in front of the wing (at the outboard spanwise location). These tests were conducted over a range of angles of attack from -10° to 110°.

SYMBOLS

C_D drag coefficient, $\frac{\text{Drag}}{qS}$

C_L lift coefficient, $\frac{\text{Lift}}{qS}$

C_R resultant-force coefficient, $\sqrt{C_D^2 + C_L^2}$

c wing chord, m

q free-stream dynamic pressure, Pa

S wing area, m^2

$V_{\ell, c}$ local flow velocity with the boom and angle of attack sensor in the calibration rig, m/sec

$V_{\ell, m}$ local flow velocity with the boom and angle of attack sensor mounted on the model, m/sec

α_m measured angle of attack, deg

α_t true angle of attack, deg

ϵ flow correction, deg

θ_s angle of wind-tunnel mounting strut, deg

TEST EQUIPMENT

Wind Tunnel

The investigation was conducted in the 12-Foot Low-Speed Wind Tunnel at the Langley Research Center. The tunnel has a 3.66-meter octagonal test section and a variable speed electric motor-driven fan. The tunnel is equipped with a movable mounting strut that can position models over a wide range of angles of attack and angles of sideslip.

Model

The model tested (fig. 1) was a fifth scale model of a low-wing general aviation airplane. The model dimensions are shown in figure 2. The model had a wing area of .36 m^2 and an aspect ratio of 6.1. The wing had a NACA 64_2 - 415 airfoil section and was untapered and untwisted with 5^o geometric dihedral per wing panel. The rear fuselage section containing the horizontal and vertical tails was removed for all of the tests. Also, the model was unpowered and did not have landing gear.

A 6.6 mm diameter cylindrical boom holding a vane angle of attack sensor was attached to the left wing of the model (fig. 1). The angle of attack sensor (fig. 3) was similar to the one reported in reference 1.

Almost all of the tests were conducted with the angle of attack sensor located 1.06 c ahead of the wing leading edge. With this length boom four spanwise boom locations on the left wing were tested (fig. 2). For one of the tests, the boom was shortened to locate the sensor .58 c ahead of the wing at the left wing tip. The outboard location, location number 1, corresponds to the boom location on the full-scale airplane involved in the stall-spin test program reported in reference 9.

Data System

Flow direction.- The angular position of the sensor was recorded using a prototype data system which is used in radio-controlled model tests at the Langley Research Center. In this system a potentiometer on the sensor produced a voltage that was proportional to the sensor position. This voltage was then used to modulate a hobby-type radio-controlled transmitter in the model. The transmitted signal was picked up by a receiver outside the test section which drove a hobby type servo to produce a meter deflection. This deflection, which was proportional to the sensor angle, was recorded manually at the different test conditions. The sensor was calibrated in the laboratory using a calibration fixture and was generally repeatable within 2°. When the sensor was used to measure the flow direction in the tunnel, the repeatability was also within 2° and was usually less than 1°.

Model force.- A three component strain gauge balance was used to obtain normal and axial forces and pitching moment for the model.

PROCEDURE

Wind Tunnel Tests

All of the wind tunnel tests were run at a dynamic pressure of 191.5 Pa. At standard sea level density this pressure corresponds to a velocity of about 17.7 m/sec and a Reynolds number, based on the wing chord, of about $.3 \times 10^6$. The test conditions are summarized in the following table (see fig. 2 for the sensor locations):

Test number	Type of test	Sensor location	α_t* range
1	Flow direction measurement	1	-10° to 110°
2	Flow direction measurement	1s	-10° to 110°
3	Flow direction measurement	2	-10° to 110°
4	Flow direction measurement	3	-10° to 110°
5	Flow direction measurement	4	-10° to 110°
6	Tunnel flow calibration	1	-10° to 110°
7	Tunnel flow calibration	4	-10° to 110°
8	Force measurement	-	-10° to 110°

*The angle of sideslip was zero for all of the tests

Wind Tunnel Flow Calibration

To account for flow irregularities in the region of the tunnel in which the model was tested a calibration was conducted. To accomplish this, an apparatus was made to position the isolated boom and sensor in the tunnel with the model removed. The apparatus was constructed so that as the wind-tunnel strut was swept through its angle of attack range, the sensor was swept through the same region of the tunnel as when the sensor was mounted on the model. With the boom and sensor in this calibration rig, the sensor angle was assumed to be equal to the true angle of attack (fig. 4(a)).

Using this equipment two tests (tests 6 and 7 in the table) were made with the sensor and boom held in positions corresponding to sensor locations numbers 1 and 4. Because the data showed little difference between the two positions the data for the boom and sensor alone in position number 1 was used as the calibration. This calibration is presented as a plot of the true angle of attack as a function of the strut angle (fig. 5).

Data Reduction

With the boom mounted on the model the sensor angle (the measured angle of attack) was measured for the various test conditions (fig. 4(b)). The flow correction, ϵ, is defined as the difference between the measured angle of attack and the true angle of attack (determined from the tunnel calibration, fig. 5) at a particular strut angle (fig. 4(c)), that is

$$\epsilon(\theta_s) = \alpha_m(\theta_s) - \alpha_t(\theta_s) \tag{1}$$

To aid the experimenter, in this report the flow correction is plotted against the experimentally determined quantity, the measured angle of attack.

RESULTS AND DISCUSSION

An example of the angle of attack data taken when the model was in the tunnel (from test 1) is shown in figure 6. The measured angle of attack at a given strut angle (from fig. 6) is plotted against the true angle of attack at the same strut angle (from fig. 5) to yield a plot of the true versus the measured angles of attack (fig. 7). This figure can be used by a flight test engineer to obtain the true angle of attack from his in-flight measurements of the angle of attack.

In order to show the actual flow correction more clearly, the tunnel flow calibration data (fig. 5) were combined with the data in figure 6 (as well as the data from tests 2-5) using equation 1. In figure 8, the flow correction for both sensor positions in front of the wing, at the outboard spanwise location, is presented. These data indicate that there is a smaller flow correction for the sensor position further from the wing. This result is probably due to the fact that the sensor is in a region of flow which is less

influenced by the wing. Figure 9 shows the flow correction at four spanwise sensor locations (all four with the angle of attack sensor located 1.06 c ahead of the wing), demonstrating that the flow correction increases as the sensor is moved inboard. This result is likely due to the variation of the lift distribution over the wing and to the increasing effect of the fuselage. At all of the sensor locations tested, the flow correction was substantial, varying from about 2° at a measured angle of attack of 0° to over 15° at a measured angle of attack of 90°.

In an attempt to correlate the flow correction with the aerodynamic characteristics of the model, the flow correction data (figs. 8 and 9) have been compared with the longitudinal force data. The lift, drag and resultant-force coefficients are plotted against the strut angle (fig. 10), which is similar to the true angle of attack (fig. 5). These data follow the general trends of the lift and drag curves of typical general aviation airplanes (ref. 10). Comparison of the force data in figure 10 with the flow correction data in figures 8 and 9 seems to indicate that the flow correction is not directly related to any one of the drag, lift, or resultant-force coefficients individually. However, at measured angles of attack above 20° the flow correction is most nearly like the drag coefficient. At the same time, the change of slope in the flow correction curves between 10° and 20° measured angle of attack may be related to the drop in lift at 10° strut angle in figure 10.

Finally, the flow correction (at position number 1) below the stall angle of attack is compared with flow correction data for a similar full scale airplane in flight (ref. 2). Figure 11 shows that the slope of the experimentally determined flow correction agrees with the slope determined in flight. However, there is a bias of about 1.5° in the flow correction at a given value of the measured angle of attack. This offset is probably partially due to a difference in the reference line between the airplane and the model. In fact, the reference line on the model was chosen arbitrarily. More tests in both the wind tunnel and flight will be needed to determine the true relationship between the two sets of measurements.

CONCLUDING REMARKS

A wind tunnel study has been undertaken to determine the nature of the flow correction for an angle of attack sensor. The sensor was mounted in front of a 1/5-scale model of a general aviation airplane. It was shown that the flow correction is substantial, varying from 2° at 0° angle of attack to over 15° at 90° angle of attack. The flow correction was found to be a function of the spanwise and chordwise location of the sensor. The correction increased as the sensor was moved closer to the wing or closer to the fuselage. The experimentally determined slope of the flow correction versus the measured angle of attack (at angles of attack below the stall) agrees closely with the slope of flight data from a full-scale airplane. However, more tests should be conducted to investigate the observed bias between the two curves.

REFERENCES

1. Kershner, David D.: Miniature Flow-Direction and Airspeed Sensor for Airplanes and Radio-Controlled Models in Spin Studies. NASA TP 1467, 1979.

2. Sliwa, Steven M.: A Study of Data Extraction Techniques for Use in General Aviation Aircraft Spin Research. Master's Thesis, George Washington University, September 1978.

3. Gracey, William: Summary of Methods of Measuring Angle of Attack on Aircraft. NASA TN 4351, 1958.

4. Wolowicz, Chester H.: Considerations in the Determination of Stability and Control Derivatives and Dynamic Characteristics From Flight Data. AGARD Report 549-Part I, 1966.

5. Alford, William J., Jr.: Theoretical and Experimental Investigation of the Subsonic-Flow Fields Beneath Swept and Unswept Wings With Tables of Vortex-Induced Velocities. NASA TN 3738, 1956.

6. Ribner, Herbert S.: Notes on the Propeller and Slipstream in Relation to Stability. NACA WR L-25, 1944.

7. Bowman, James S.; Stough, H. Paul; Burk, Sanger M.; and Patton, James M.: Correlation of Model and Airplane Spin Characteristics for a Low-Wing General Aviation Airplane. AIAA Paper No. 78-1977, August 1978.

8. Sliwa, Steven M.: Some Flight Data Extraction Techniques Used on a General Aviation Spin Research Aircraft. AIAA Paper No. 79-1802, August 1979.

9. Patton, James M.; Stough, H. Paul; and DiCarlo, Daniel J.: Spin Flight Research Summary. SAE Paper No. 790565, 1979.

10. Bihrle, William, Jr.; Barnhart, Billy; and Pantason, Paul: Static Aerodynamic Characteristics of a Typical Single-Engine Low-Wing General Aviation Design for an Angle-of-Attack Range of -8^{o} to 90^{o}. NASA CR 2971, 1978.

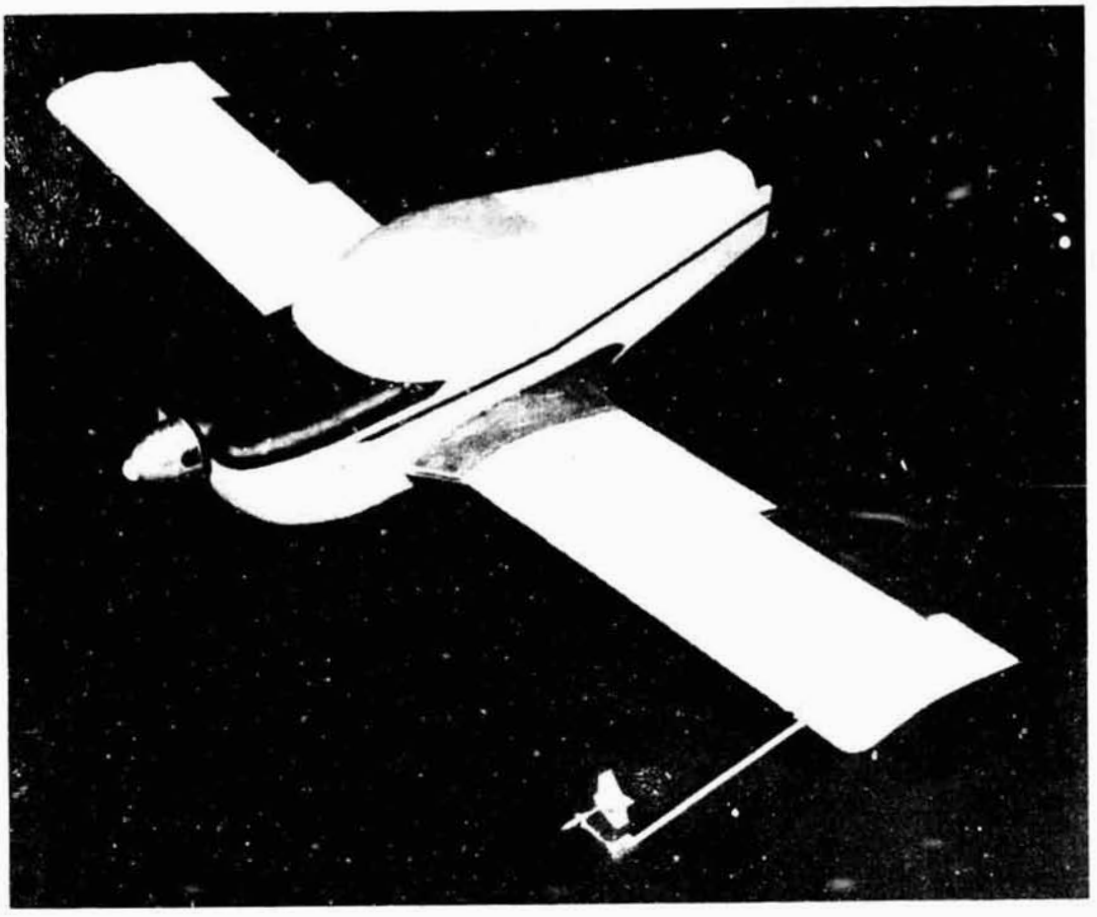

Figure 1. - Photograph of the model.

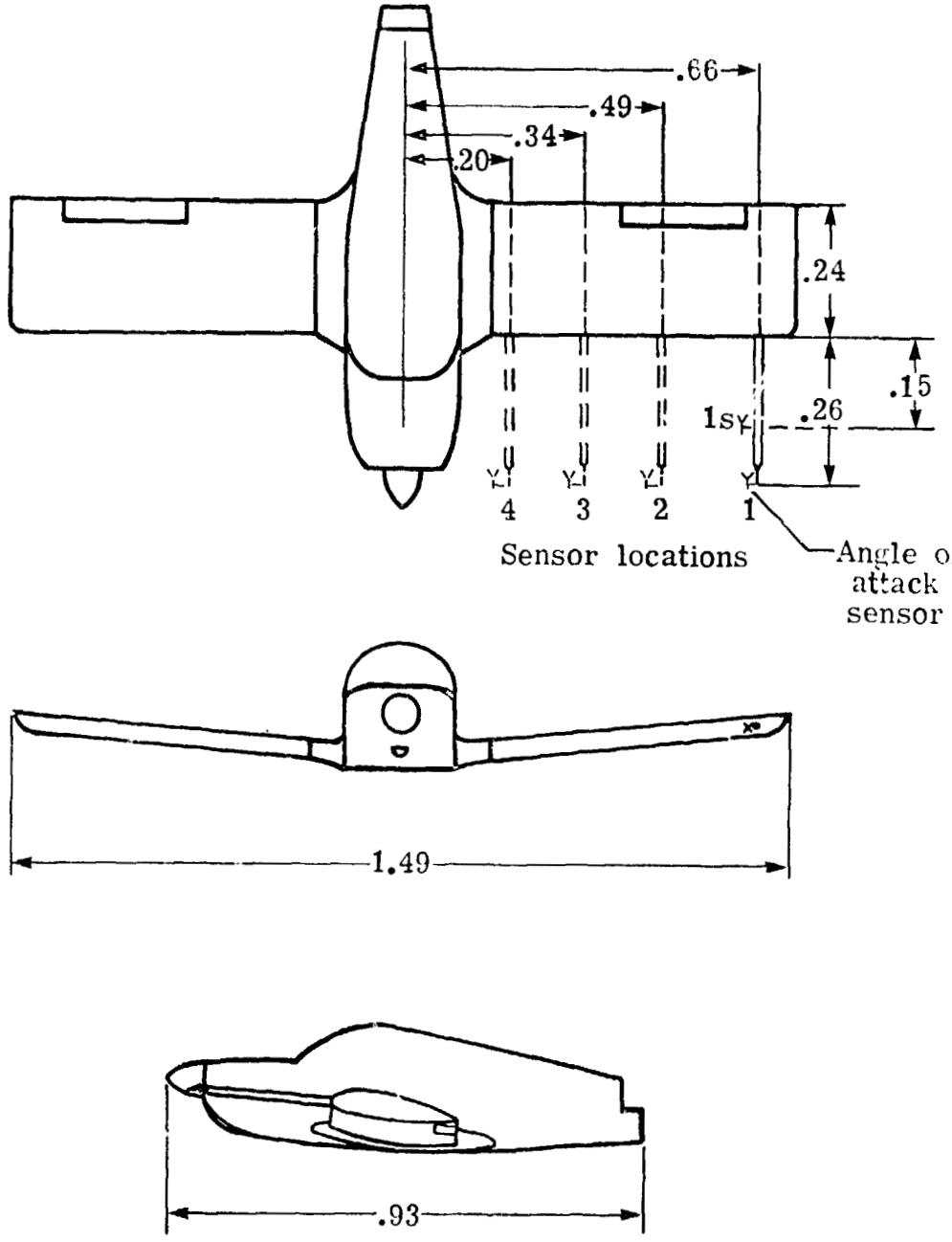

Figure 2.- Three-view drawing of the model showing the sensor locations tested. All dimensions are in meters.

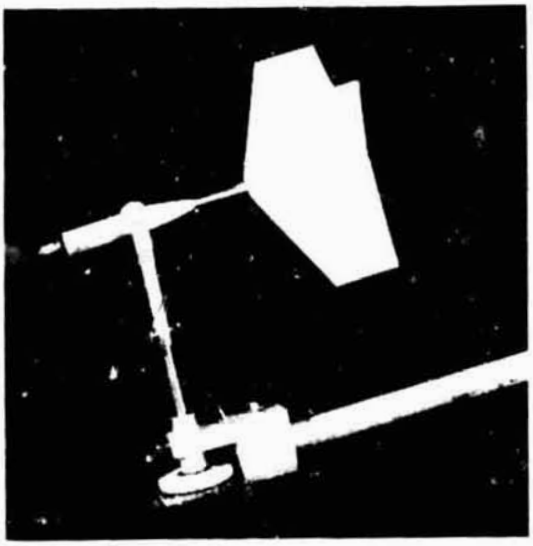

(a) Photograph of the angle of attack sensor.

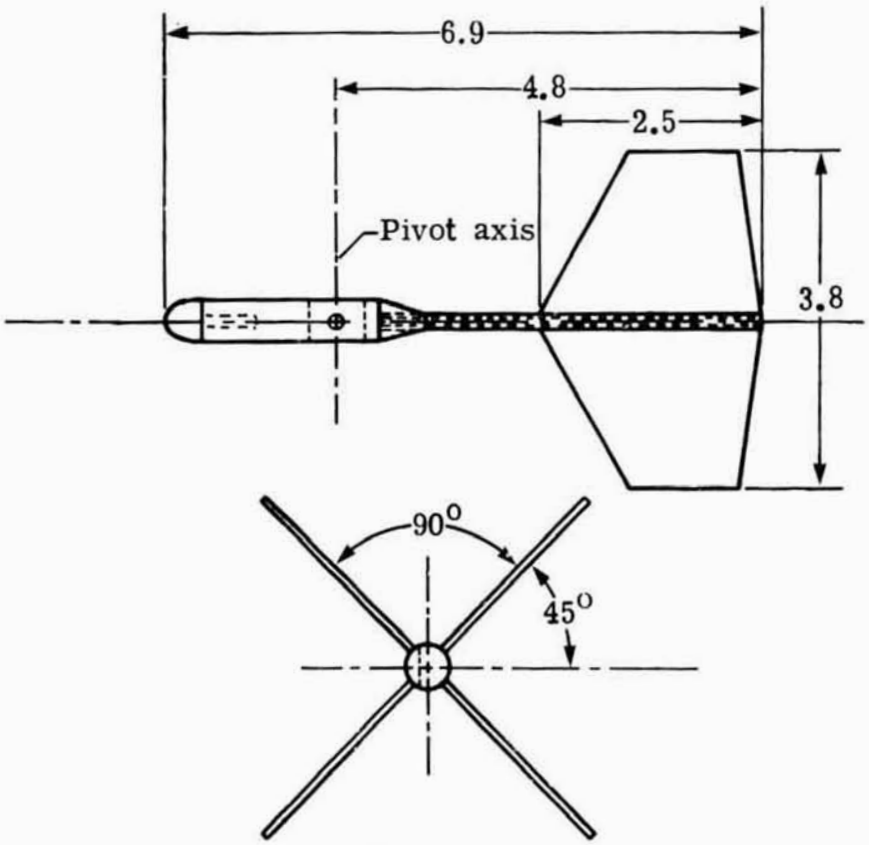

(b) Dimensions (in cm) of the angle of attack sensor.

Figure 3.- Photograph and dimensions of the angle of attack sensor.

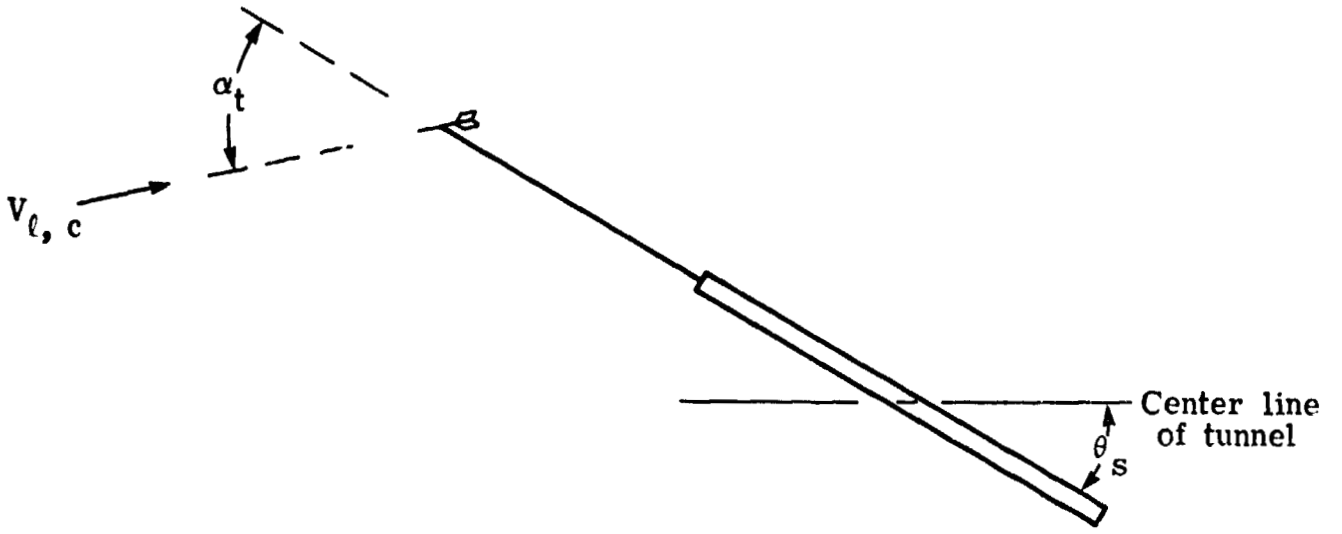

(a) Tunnel flow calibration.

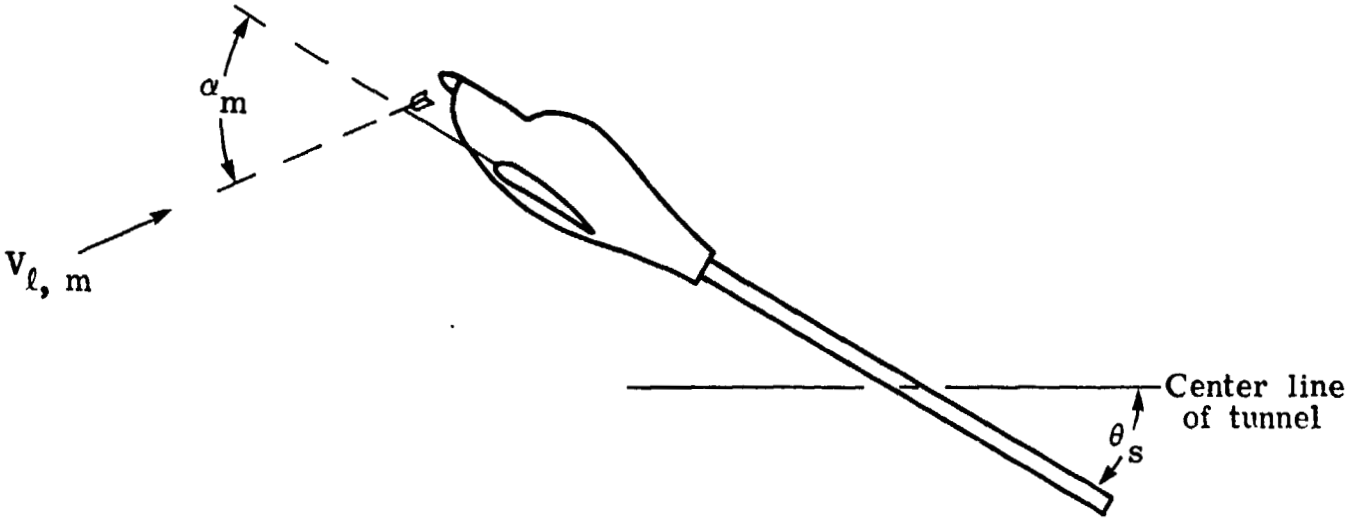

(b) Flow direction measurement.

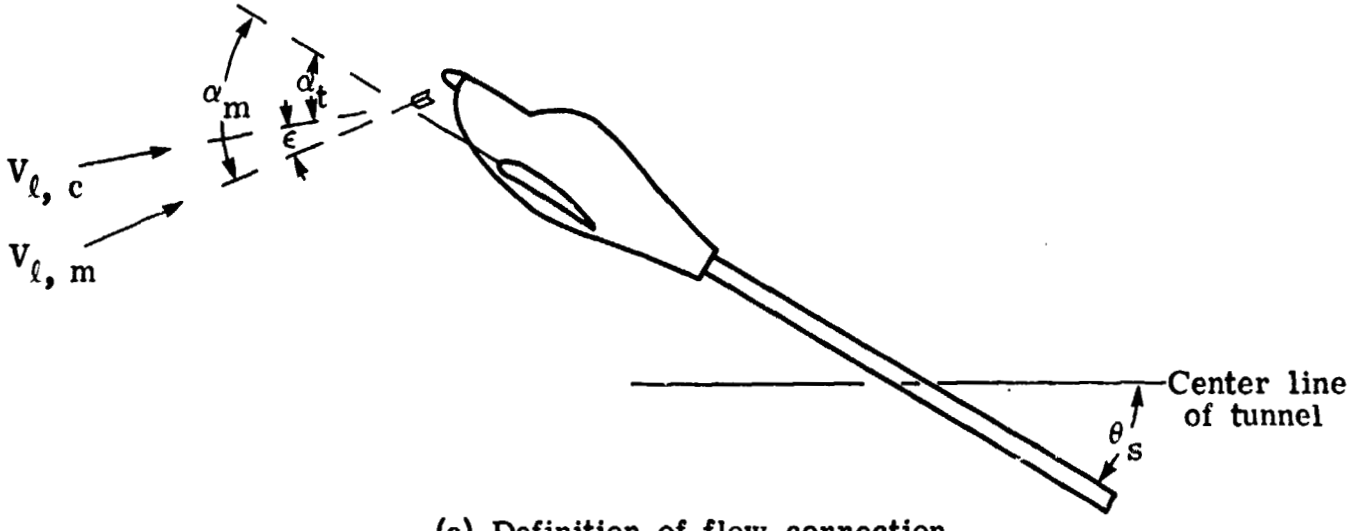

(c) Definition of flow correction.

Figure 4.- Definitions of the angles measured to determine the flow correction.

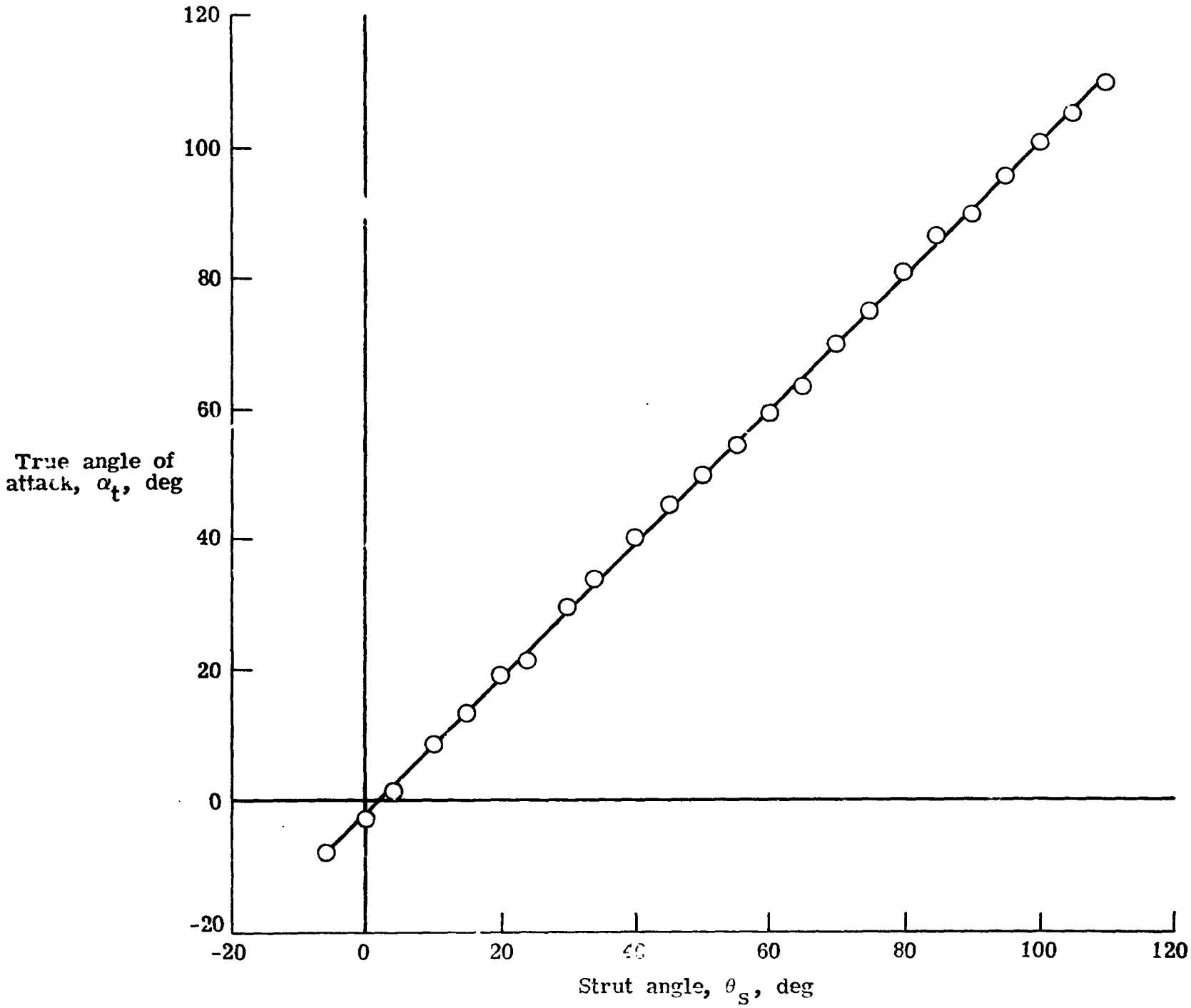

Figure 5.- Wind-tunnel flow calibration.

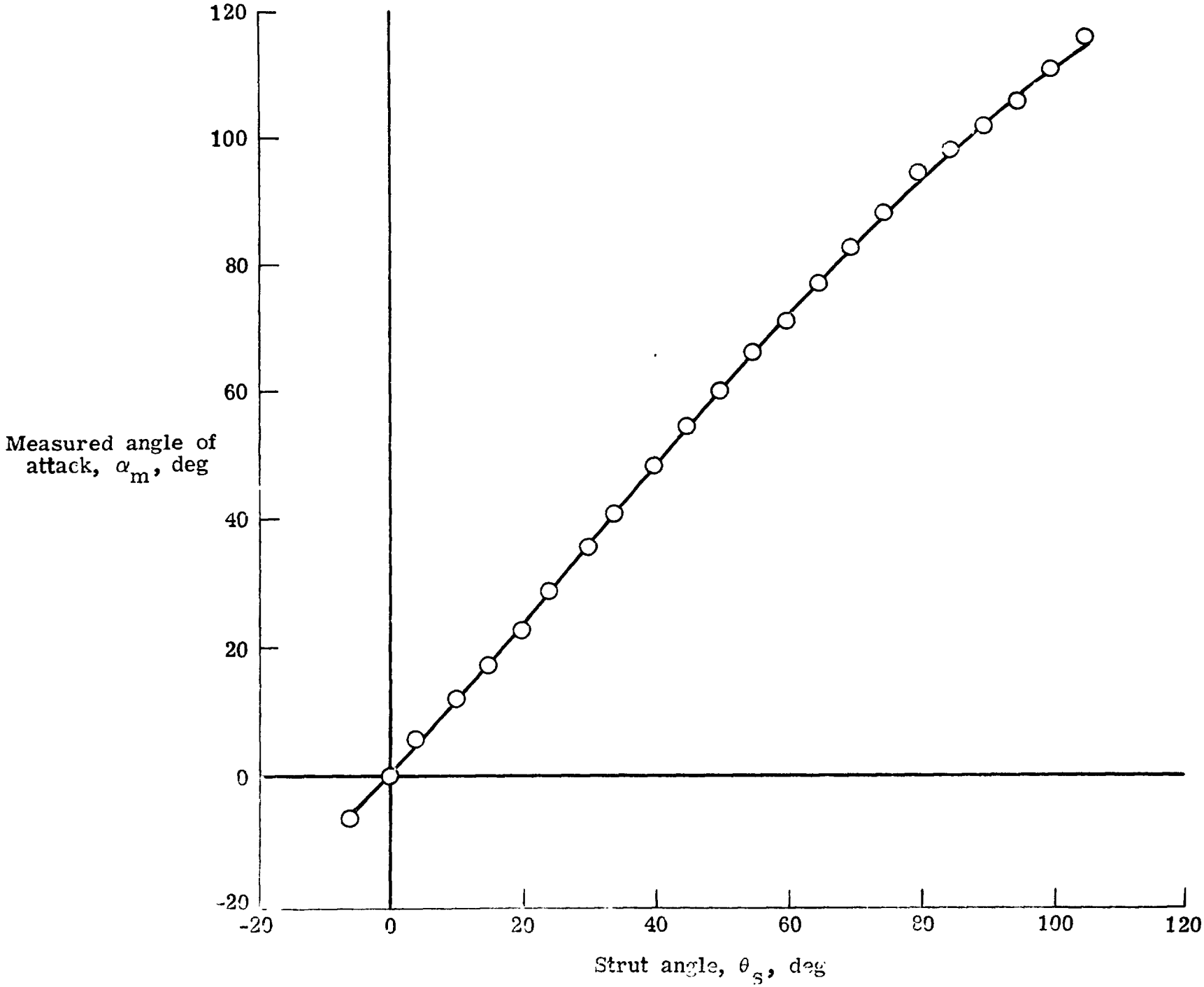

Figure 6.- Measured angle of attack at sensor location #1.

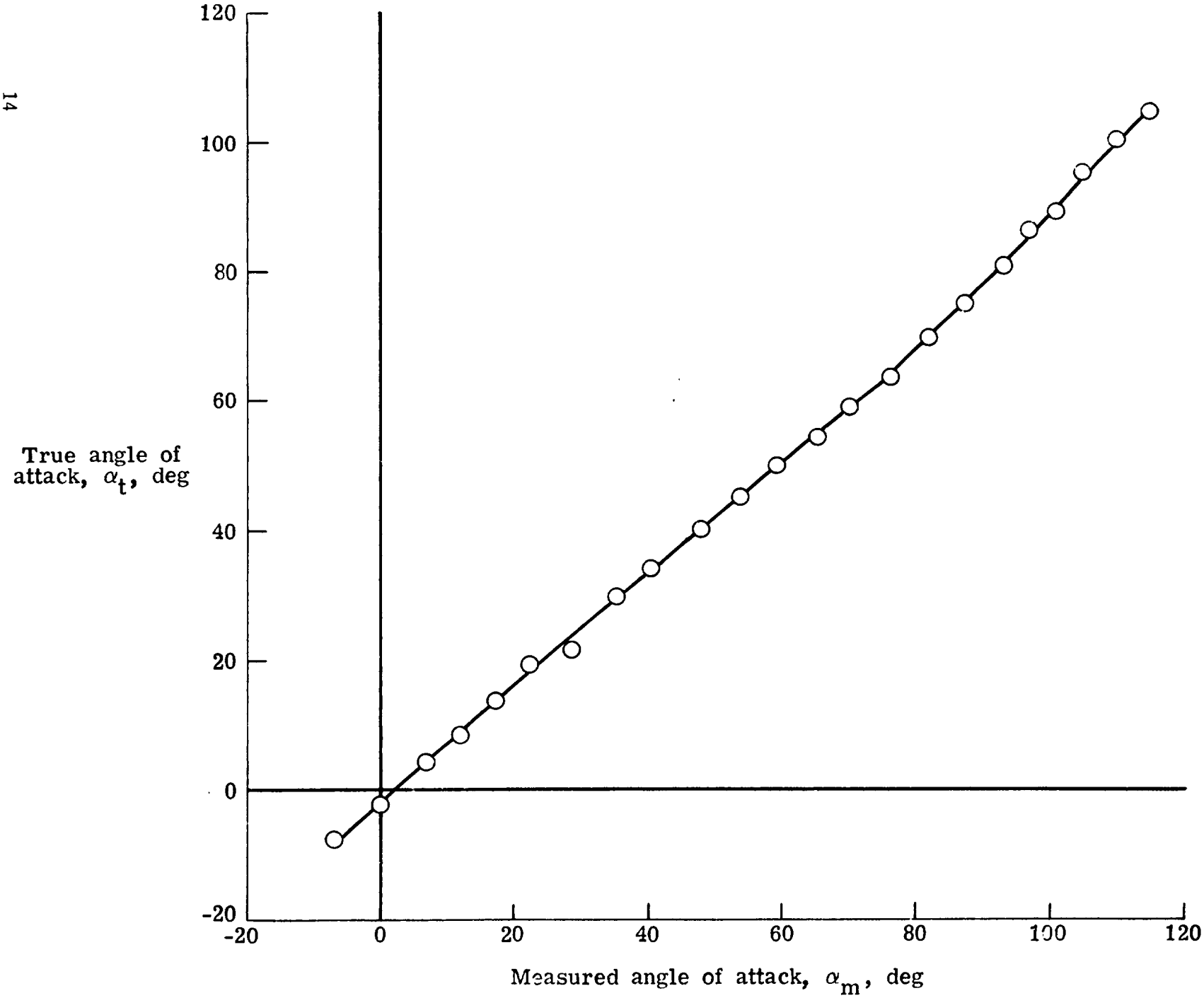

Figure 7.- The true angle of attack as a function of the measured angle of attack.

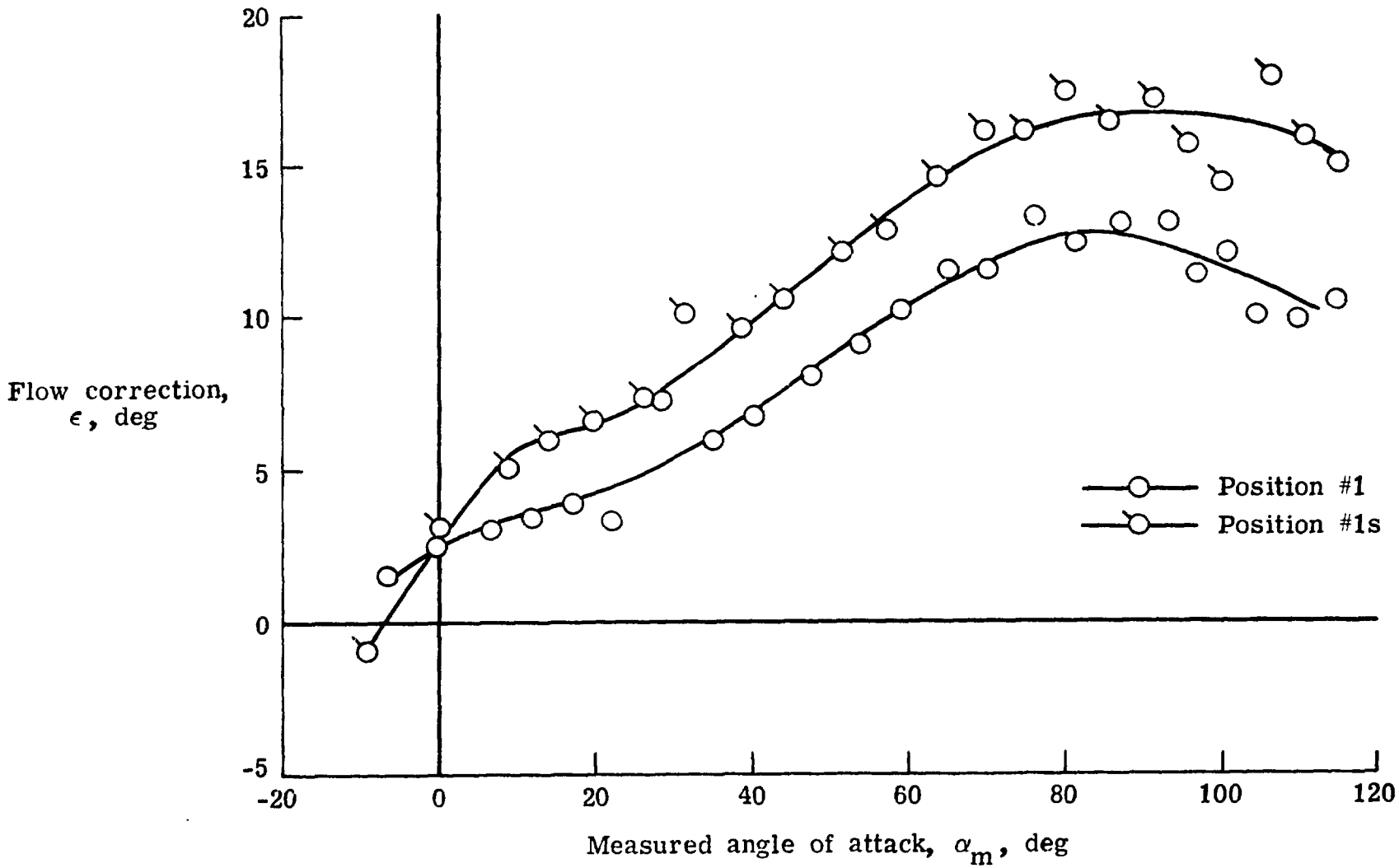

Figure 8.- The effect of the chordwise location of the sensor on the flow correction.

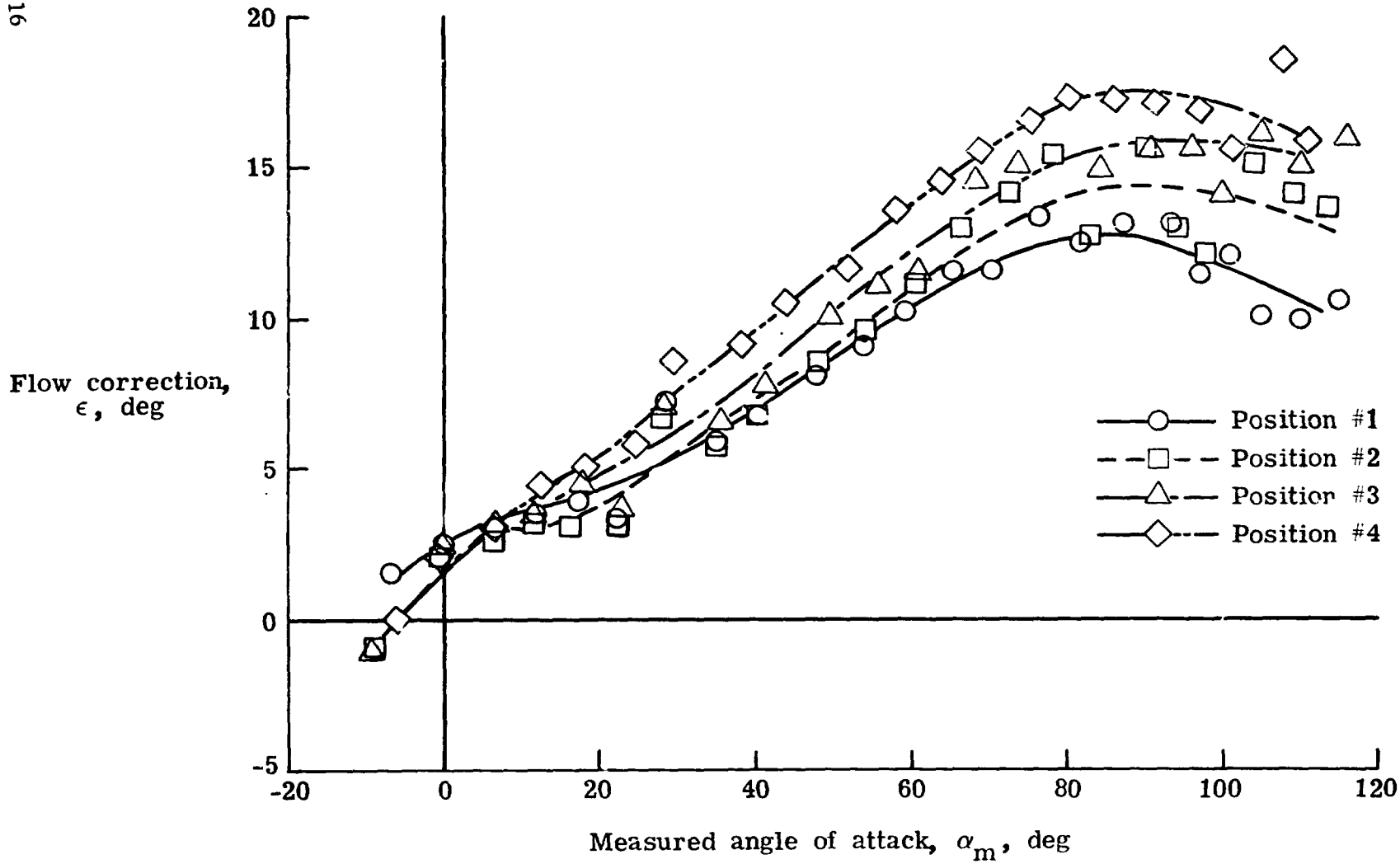

Figure 9.- The effect of the spanwise location of the sensor on the flow correction.

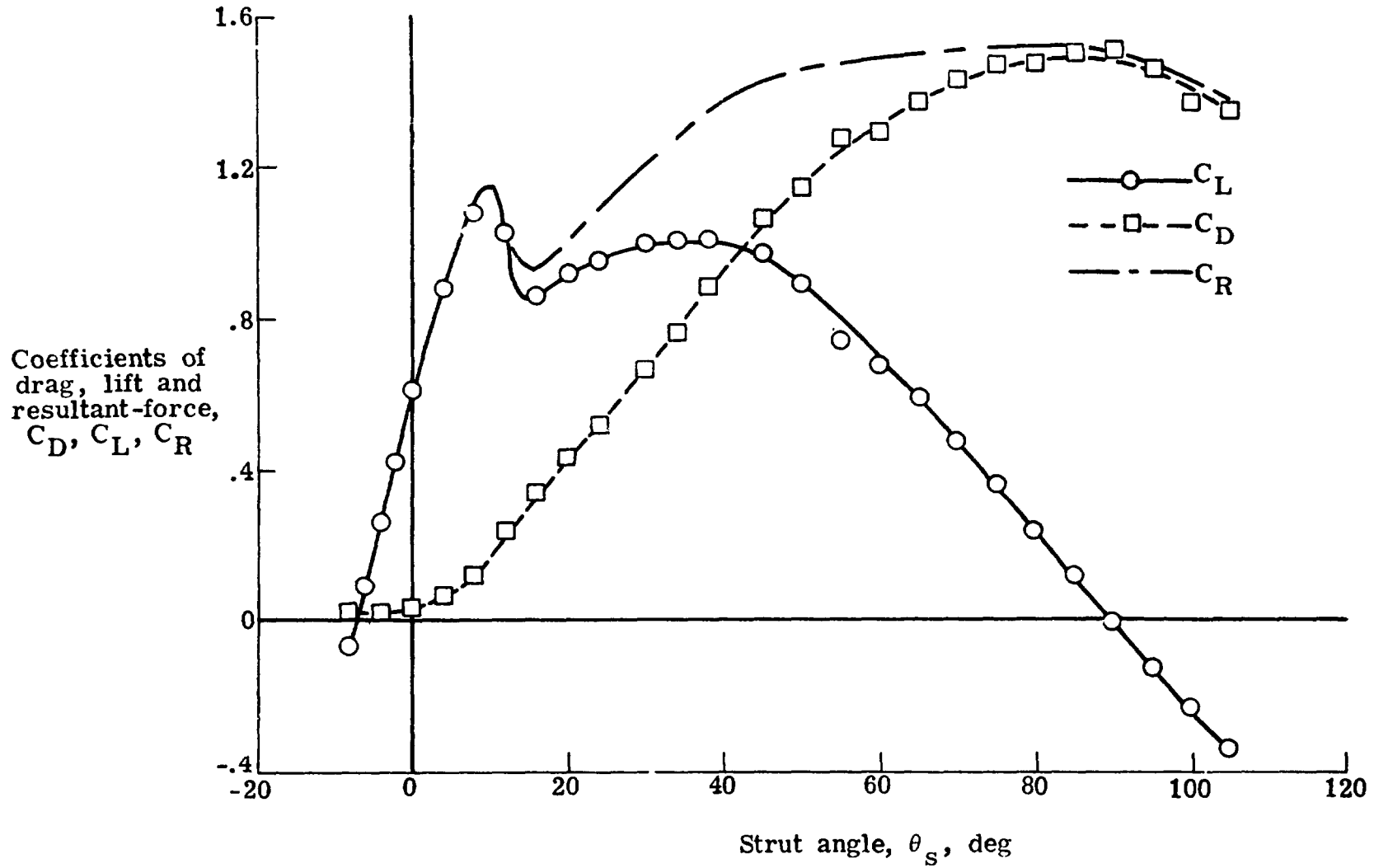

Figure 10.- Longitudinal force data for the model.

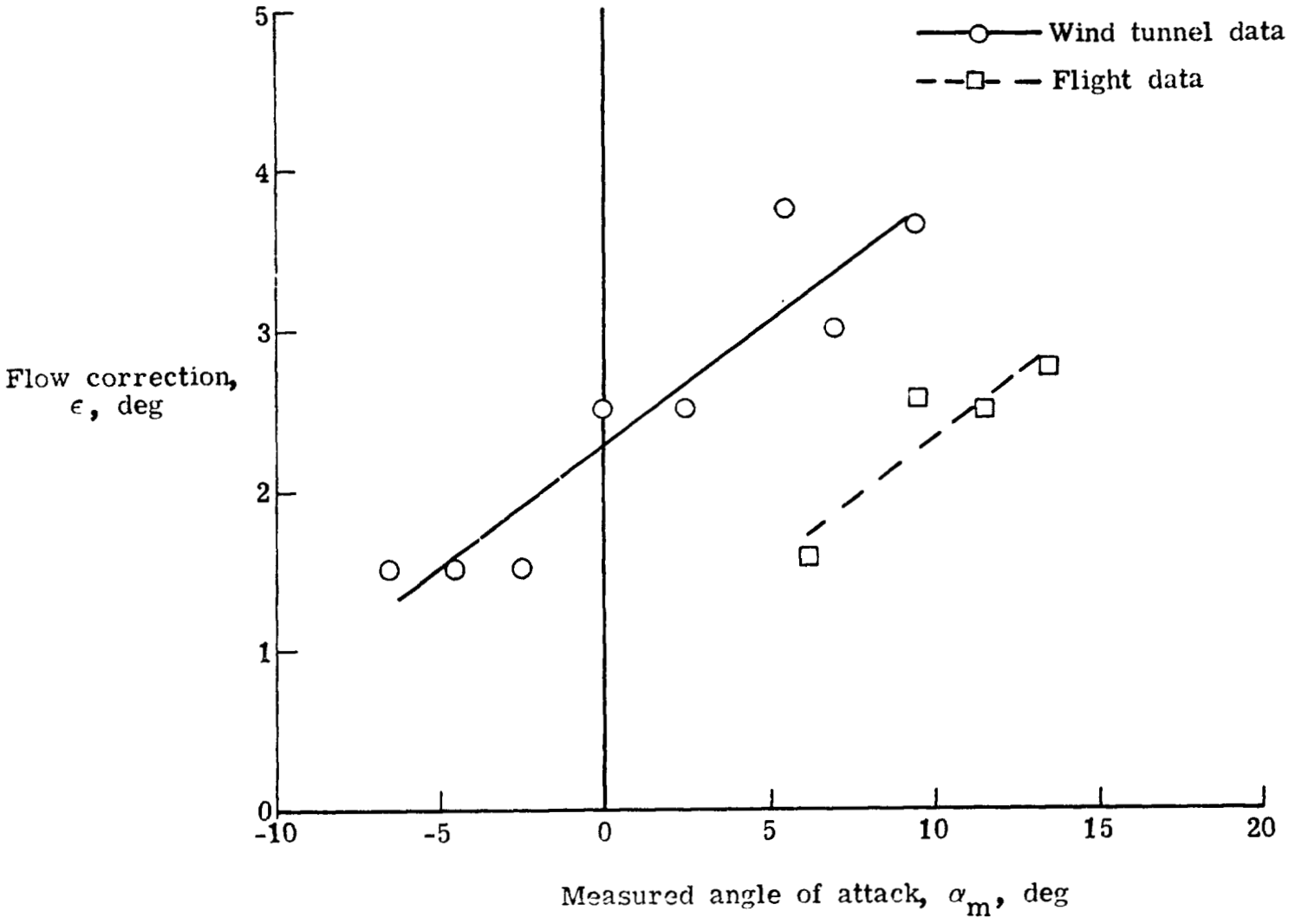

Figure 11.- Comparison of the experimentally determined flow correction with flow correction data for a similar full scale airplane in flight.